Original Research Paper

IJES *Iranian Journal of Earth Sciences*
Vol. 14, No. 1, 2022, 40-57.
DOI: 10.30495/ijes.2022.1929200.1601

Petrology and tectono-magmatic environment of the volcanic rocks of West Torud – Iran

Abdollah Yazdi*[1], Elham Shahhosini [2], Farhad Moharami [3]

1. Department of Geology, Kahnooj Branch, Islamic Azad University, Kahnooj, Iran
2. Young Researchers and Elite Club, North Tehran Branch, Islamic Azad University, Tehran, Iran
3. Department of Geology, Payame Noor University, Iran

Received 11 May 2021; accepted 3 November 2021

Abstract

Middle-Upper Eocene volcanic and volcano-sedimentary rocks of the Torud region have been formed by the sequences of basic-intermediate lavas, pyroclastic rocks, and sedimentary layers (e.g., siltstone, sandstone, and nummulite-bearing limestone) within a shallow marine basin. According to microscopic studies, the volcanic rocks of the region include basalt, basaltic andesite, trachyandesite, andesite, and dacite. These rocks have originated from the differential crystallization processes and occasionally calc-alkaline contamination geochemical properties. Generally, they contain olivine, clinopyroxene, and plagioclase ± amphibole minerals. Porphyritic to megaporphyritic textures with microlithic and flow matrixes are observed in these rocks. Studying the main and rare elements of these rocks indicates that reducing MgO content is accompanied by an increase in Al_2O_3, K_2O, Na_2O, and SiO_2 and a decrease in Fe_2O_3 and CaO concentrations. These rocks are mainly enriched in LIL and LREE elements but depleted of HFS elements. The prominent features of these rocks are the presence of positive anomalies in the K, Sr, Rb, and Ba elements, the depletion of some samples of Nb and Ta, and their depletion of Ti and P. This result reveals the crustal contamination of the mantle mafic magma constructing these rocks. According to the geochemical data, magmatic pollution has not been an effective process in the formation of these rocks. In addition, the relatively higher levels of Cr, Ni, and MgO in the alkali basalts of the region indicate that these rocks are originated from partial melting (5 to 10%) of a spinel-garnet peridotite. Overall, they have no subduction-dependent rock characteristics and mainly represent characteristics of alkali basaltic magmas of the preliminary back-arc basin (BAB). These features, attributed to their calc-alkaline nature, represent the formation of these rocks in a tectonic back-arc setting in the Middle-Upper Eocene.

Keywords: *Petrology; Geochemistry; Volcanic rocks; Eocene; Back-arc; Torud*

1. Introduction

In Iran, Paleogene volcanic rocks crop out in three general regions (Fig 1). The first is along an NW-SE belt that extends about 1500 km across the central part of the country. This belt terminates rather abruptly to the southeast near the Pakistan border and merges with volcanic rocks in the Lesser Caucasus and Alborz Mountains to the northwest. The belt is subparallel to and approximately 175-200 km northeast of the Main Zagros reverse fault. However, Neogene NE-SW shortening within the Sanandaj-Sirjan zone may have lessened this gap since the time of active subduction (Berberian and Berberian 1981). The Lesser Caucasus/Alborz belt extends southeast to near Semnan, wherein it becomes discontinuous and extends into eastern Iran. The third region is a large area of Tertiary volcanic rocks in the Lut block of eastern Iran (Jung et al. 1984). Paleogene magmatism and extension were driven by an episode of slab retreat or slab rollback following a Cretaceous period of flat slab subduction, analogous to the Laramide and post-Laramide evolution of the western United States (Verdel et al. 2011). The study region with an area of 70 km^2 is located 120 km south of Shahroud city and 70 km southeast of Semnan (Iran) at 54° 30′ to 55° 00′E and 35 ° 15′ to 35´N within the northern part of the Central Iran zone. The area has been investigated by several researchers such as, Reuter et al. (2007), Kasmin and Tikhonova (2008), Verdel (2009 and 2011), and Bin and Meiyin (2010). In these studies, the tectonic setting of Torud Basin has been considered a preliminary immature back-arc tensile basin with an age of the Oligocene-Miocene period in the main magmatic back arc of Urmia-Dokhtar (Fig 1).

2. Study Method

A total of 175 samples were collected from the igneous rocks of the Torud complex. Next, 150 thin sections were prepared from these samples and studied by a polarized microscope. Afterward, 20 representative samples were selected for whole-rock chemical analysis (Table 1 and 2). Samples weighed between 1 and 1.5 kg before crushing and powdering. Whole-rock major elements were determined by an X-Ray fluorescence (XRF) spectrometer. Finally, trace and rare earth elements (REEs) were determined by lithium metaborate fusion ICP-MS at the GSI laboratory in Tehran, Iran.

*Corresponding author.
E-mail address (es): Yazdi_mt@yahoo.com

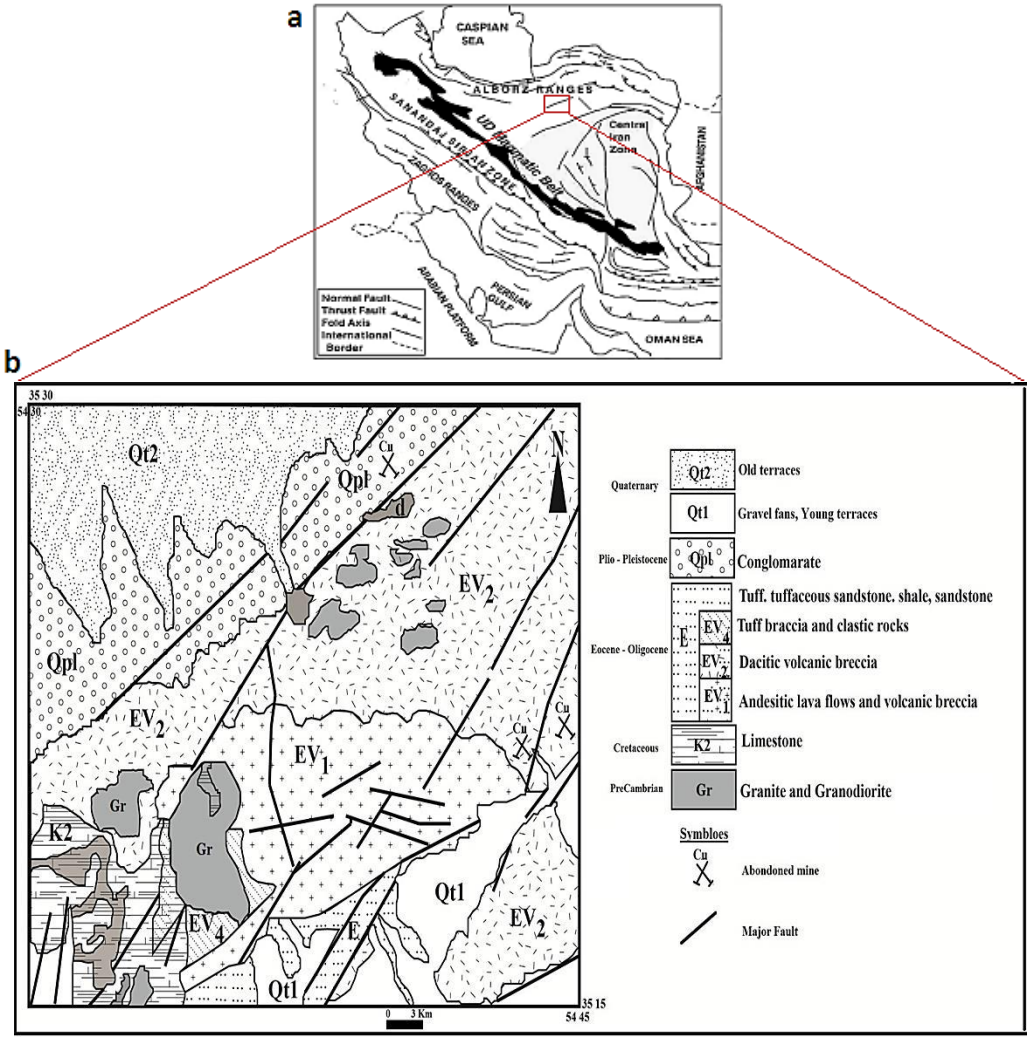

Fig 1. a) The study area in the map of structural zones in Iran (Gile et al. 2006); b) The location of the studied area in the Central Iran zone in 1:100000 map of Torud (Hooshmandzadeh et al. 1978).

3. Geological setting

The Central Iranian Plateau is located northeast of the Zagros-Makran Neo-Tethyan suture and its subparallel Cenozoic magmatic arc between the convergent Arabian and Eurasian plates. Thus, due to the collision setting, continuous continental deformation processes affect Central Iran. This plateau was a stable platform during Paleozoic times, but late Triassic movements caused the creation of horsts and grabens. Central Iran comprises three major crustal domains: the Lut Block, the Kerman-Tabas Block, and the Yazd Block. The plateau is surrounded by faults and fold-and-thrust belts and Upper Cretaceous to Lower Eocene ophiolite and ophiolitic mélange (Davoudzadeh 1997). Adjacent fault-separated areas and tectonic units are the Alborz and Kopeh-Dagh region (which ranges to the north), Makran and Zagros (which ranges to the west and south), and the East Iran Ranges (which borders this plateau to the east). The structural components (Lut Block, Kerman-Tabas, and Yazd) of the Central Iranian Plateau are characterized by distinct horst (e.g., Lut block) and graben (e.g., Kerman-Tabas region) structures. The grabens are characterized by fillings of thick Jurassic sediments. However, the stratified cover rocks are largely correlatable among these blocks, but with locally significant facies and thickness variations across the block boundaries. The blocks are characterized by an individual deformation style and seismicity, making them distinguishable from the adjacent regions (Berberian and King 1981). Central Iran has undergone severe changes during the Mesozoic and Tertiary periods. These movements were accompanied by folding, uplift processes, metamorphism, and magmatism (Aghanabati 2004; Yazdi et al. 2016). The magmatic activities in central Iran have occurred in several main stages, including Upper Eocene-Oligocene, Oligocene-Miocene, and Pliocene (Eshraghi 2006). Magmatic activities in the Moaleman-Torud occurred

during the Upper Eocene stage. After orogenesis in the Late Cretaceous, a large amount of basalt, andesite (Figs. 3a and 3b), dacite, and rhyolite were deposited in the Eocene period. These depositions were accompanied by pyroclastic and clastic sediments in the Karaj formation in central Iran and Alborz.

3.1. Petrographic studies

Based on the study of 135 prepared samples, the volcanic rocks in the study area, according to mineral assemblages, can be divided into five sub-groups: (I) Olivine basalt with grey to greyish brown colors, which displays vitrophyric, porphyritic, and intersertal textures. Plagioclase, olivine, and clinopyroxene have formed the main phenocryst phases in these basaltic rocks. The microcrystalline matrix is dominated by plagioclase, clinopyroxene, and olivine (Figs. 3c and 3d). (II) The second subgroup includes olivine trachybasalt to trachybasalt with porphyritic and trachytic textures. These samples contain plagioclase, clinopyroxene, biotite, and olivine. Their groundmass consists of plagioclase, pyroxene, apatite, and opaque minerals. (III) The third subgroup includes trachyandesites, which are dark grey to black and have trachytic, porphyritic, and microlithic textures. Plagioclase, clinopyroxene, and biotite are ubiquitous phenocrysts. The groundmass consists of plagioclase and biotite microliths with minor clinopyroxene. (IV) The fourth subgroup includes pyroxene andesites to hyalo pyroxene andesite with porphyritic and flow, glomeroporphyritic, and sieve texture. These samples contain plagioclase and clinopyroxene. In andesitic rooks, plagioclase is often decomposed into sericite, chlorite, and clay minerals. Secondary quartz is also in the form of fine granules in the matrix and sometimes filler of rock drills. In andesitic rocks, magnetite and titanomagnetite (opaque minerals) are accessory minerals, and apatite is the secondary mineral (Figs. 2e and 2f). (V), finally, the fifth subgroup includes dacites with pink to gray colors, which display spherulitic, porphyritic, and flow textures. These samples contain plagioclase, alkali feldspar, biotite, and quartz with accessory zircon, opaques minerals, and apatite. Chlorite, sericite, and clay minerals are the alteration products of the original minerals.

Based on petrographic features, there are three types of plagioclases in the volcanic rocks of the area:

1. Without sieve texture mostly lacking zoning with a clear border with the rock background
2. With sieve texture at the center and with a growing ring of intact and clear plagioclase
3. With solubility margins and a relatively intact crystal center (Fig 3)

The existence of non-equilibrium textures in plagioclase suggests the physicochemical changes of magma during cooling (Vernon 2004).

Sieve textures have formed due to two major causes:

First, during the pressure reduction processes (Nelson and Montana 1992): During this process, when the magma is saturated with high velocity climbs into lower depths, the vapor pressure of the system increases. The stability of the plagioclase crystals decreases, and crystalline dissolution filled with molten cavities occurs (Blundy and Cashman 2005). After crystallization of the crystalline crystallization, these cavities are enclosed within the crystal, and the sieve texture is formed in the crystal. Sieve texture resulting from this process is of large size (Nelson and Montana 1992). Large coagulants are observed in the center of plagioclase phenocrysts. Stewart and Pierce (2004) argue that the instability of plagioclase crystals during the fast upward movement of magma causes the formation of sieve texture in them. Due to partial melting in some parts of the plagioclase, the melting products inside the crystal begin to crystallize. Whether the temperature decline is rapid or slow, these products crystallize in the form of a glass or new plagioclase inside the primary plagioclase, leading to the emergence of sieve texture.

Second, magmatic mixing or reaction with high-temperature calcium-rich molten magmatic stores occurs at lower depths. Therefore, the phenocrysts tolerate dissolution in interaction with high-calcium molten liquid (Ghaffari et al. 2013 and 2015). After the dissolution, the crystals react in a new condition to stabilize the molten state and recrystallize. The size of the sieve produced by this process is small. In this respect, studies have shown that anorthite-rich plagioclase crystals form in high temperature, low pressure, and high- Ca/Al, Al/Si, Ca/Na low water content (Nelson and Montana 1992; Blundy and Cashman 2005).

Zoning is one of the other non-equilibrium textures observed in the plagioclase is in the rocks of the region (Fig 3). This structure is attributed to two main causes: 1) crystallization of plagioclase from a melt undergoing continuous variations in temperature, water vapor pressure, and composition (Humphreys et al. 2006) and 2) increasing the growth rate of the crystalline-molten joint in response to equilibrium conditions (Ginibre et al. 2002). In a magma reservoir, magma is affected by dynamic activities such as convective flows or the entry of very hot calcium-rich magma, or both. Following the effect of these processes, textures such as small sieve, zoning, and dissolution have formed, and the facial shape is either in the margin of the previous crystals (Singer et al. 1995; Yazdi et al. 2019). In the long term, the crystal inside the molten is usually balanced between plagioclase and magma composition with no zoning. Conversely, the presence of a zoning structure indicates a slowdown in the speed of equilibrium with respect to the crystallization rate (Shelly 1993). Therefore, the presence of zoning in plagioclase seems to be due to the rapid cooling of the mass margin and possibly due to rapid temperature changes.

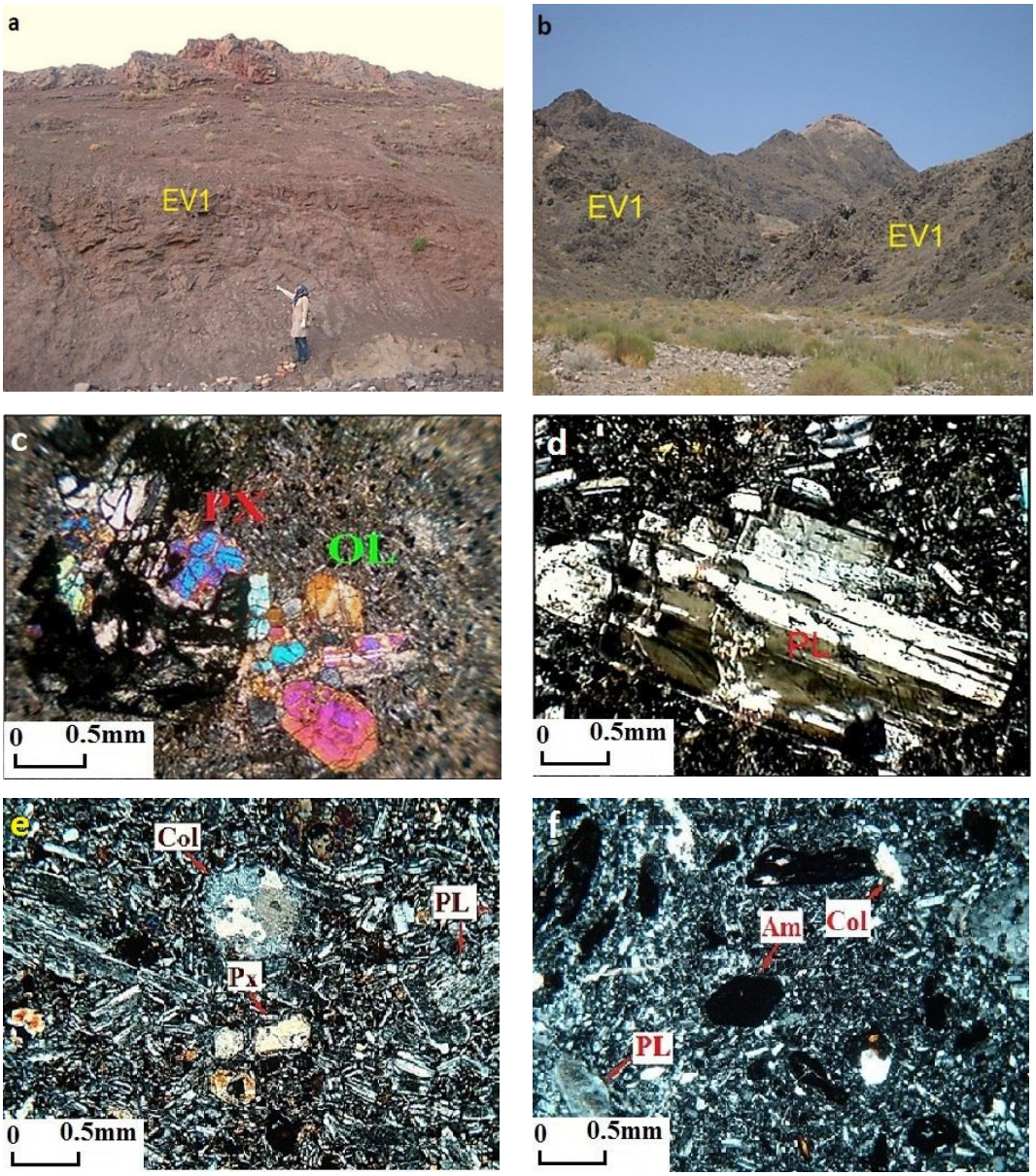

Fig 2. a) The presence of andesitic rocks in the southwest of Torud village; b) The volcanic rocks in the west of Torud; c) Accumulation of olivine and clinopyroxene crystals in olivine-basalts and formation of glomeroporphyritic textures in olivine-basalt; d) The bay corrosion, sieve, and skeletal textures in plagioclase crystals in trachy basalt; e) The altered plagioclase phenocryst and calcite-filled amygdaloid cavity in pyroxene andesite; f) The plagioclase phenocrysts, opaque amphiboles, and chlorite filling the voids in trachyandesite.

3.2. Geochemical studies of volcanic rocks in the area

Investigating the main elements of volcanic rocks in the west of Torud indicates that these rocks are within a range of intermediate basic volcanic rocks (Table 1 and 2). The SiO_2 contents in these rocks range from 48 to 65% (Table 2). According to the TAS diagram shown in Fig 3, they can be classified into 4 groups of basalts, trachyandesite andesitic basalts, trachyandesites, and dacite. Also, based on the geochemical classification diagrams shown in Figs. 3a and 3b, the composition of the studied samples is in the range of sub-alkaline basalt, alkaline basalt and andesite, trachyandesite, and dacite, which is in good consistency with petrographic studies. In the (Na_2O + K_2O)-SiO_2 diagram (Irvine and Baragar 1971), the samples are in the sub-alkaline range, while in the diagram of Hastie et al. (2007), they mainly fall in the shoshonitic to the calc-alkaline zone. The shoshonites are divided into three categories of basic (SiO_2 < 53 wt.%), intermediate (SiO_2 = 53-63), and acidic (SiO_2 > 63 wt.%) (Morrison 1980). These rocks are mainly found in subduction-related tectonic environments.

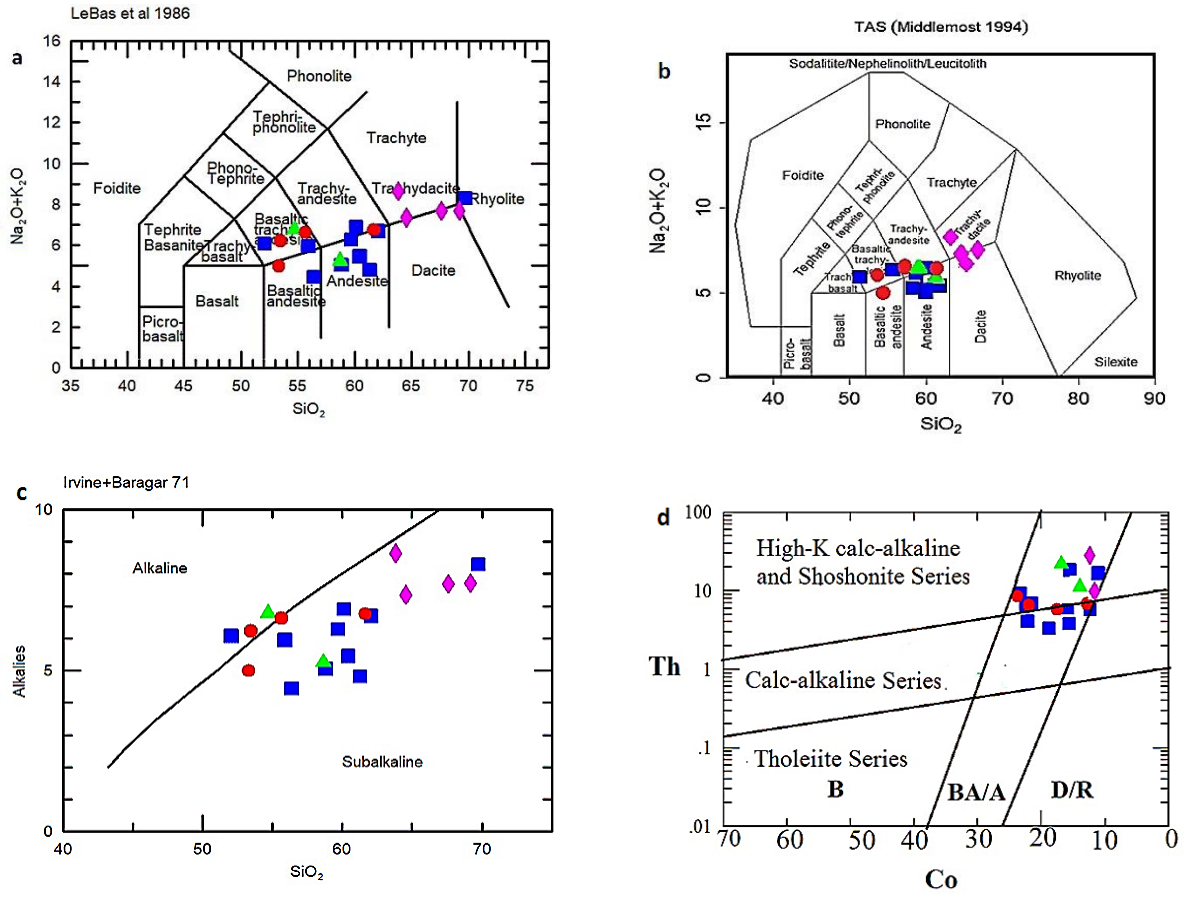

Fig 3. a) The location of the samples in the diagram of SiO_2 versus K_2O + Na_2O (Lebas et al., 1986); b) The Middelmost's diagram (1994); c) The (Na_2O+K_2O)- SiO_2 diagram of Irvine and Baragar (1971); d) The diagram of Th-Co rare elements (Hastie et al. 2007) to separate the Tholeiitic and calc-alkaline ranges and the position of the samples in the area; basalt: B, basalt-andesite: BA/A and dacite and rhyolite: D/R.

Basalt: ● Andesite: ■ Trachy andesite: ▲ Dacite: ◆

The shoshonites are the products of magmatic activity above subduction zones in continental arcs, post-collisional arcs, or in oceanic-arc settings where potassic rocks are related to the melting of phlogopite-bearing mantle wedge (Morrison 1980, Peccerillo 1992, Müller and Groves 1997).

A slight tendency toward the alkaline nature in basalts may be due to contamination with crustal materials or materials with a back-arc basin origin (Figs. 3b and 3c).The variations of the main elements against MgO are represented in Fig 4. As can be seen, the contents of the main elements, i.e., Al_2O_3 and SiO_2, increase by decreasing MgO during magmatic subtraction. However, the main elements such as CaO and Fe_2O_3 reduce by decreasing MgO levels. This declining trend of Al_2O_3 and SiO_2 concentrations against MgO indicates the fractional crystallization of preliminary olivine compared to plagioclase crystallization in the liquidus phase. Increasing MgO by CaO and Fe_2O_3 (t) denotes the importance of pyroxene crystallization in rocks in the area. The diagram of rare element changes against Zr and Th is an appropriate tool to interpret the magmatic evolution trend. Zr is a proper element for use in change diagrams because of its very low mobility during alteration and wide changes in basalts (Le Roex et al. 1983; Widdowson 1991; Widdowson et al. 2000; Talusani 2010; Meng et al. 2012). In addition, this element displays completely incompatible geochemical behavior during partial melting and differential crystallization in basaltic melts (Talusani 2010) and has a strong tendency to enter and remain in the melt phase. As seen in Fig 4, the correlation between Th and Zr is linearly positive; however, Sm relative to Zr is somewhat scattered and positive. The Ni toward Zr trend is scattered but negative, and Th against Hf is relatively scattered and positive. The trends observed in these diagrams represent the relationship of the rocks in the region and suggest an origin magma for them with almost similar geochemical properties. Besides, the main petrological control of these rocks is related to the crystallization process in the basaltic magma of the area. Nevertheless, their scattering is attributed to the abundance of mafic phenocrysts and plagioclases.

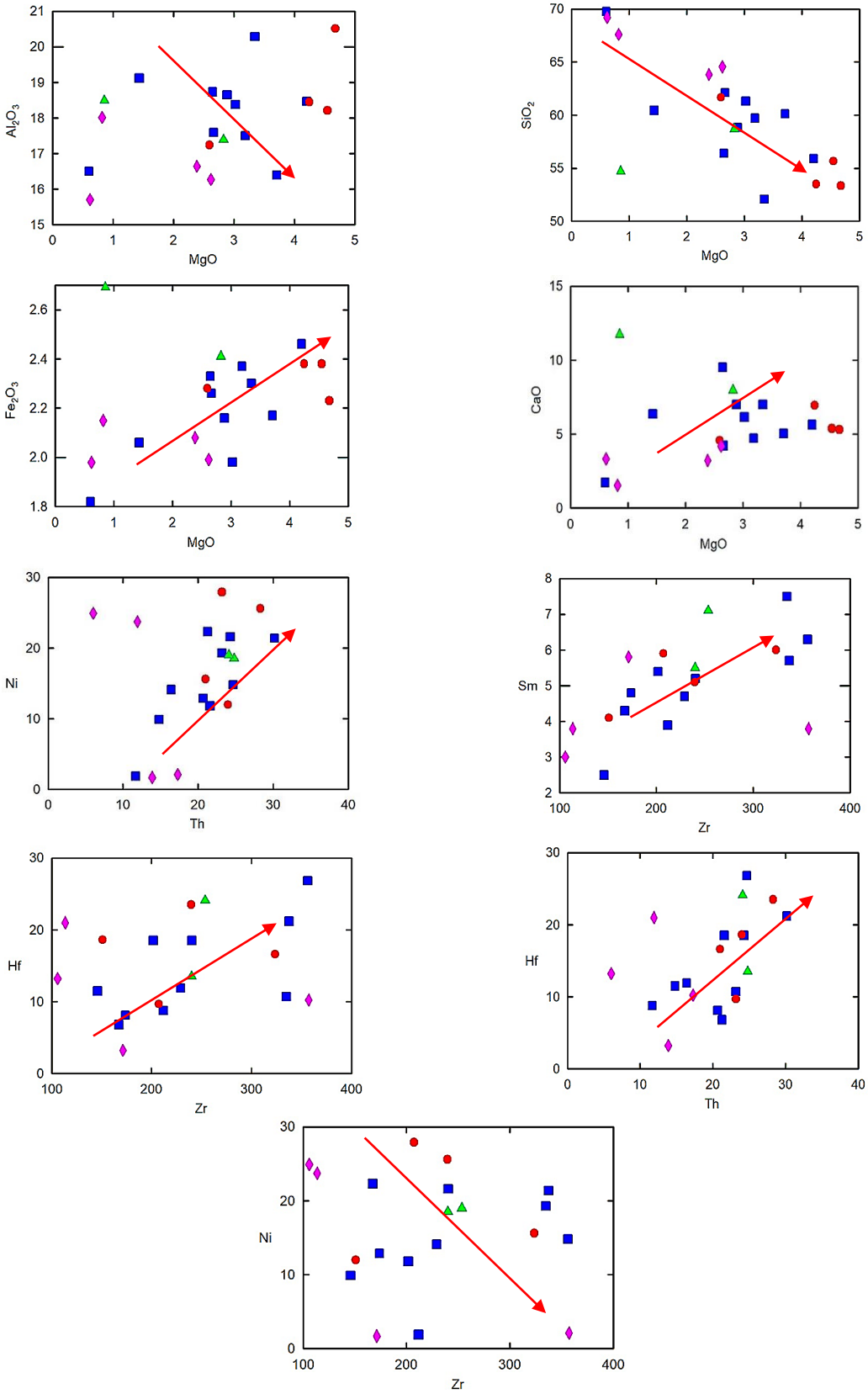

Fig 4. The trend of main elements changes against MgO and rare elements against each other

The samples studied in the normalized diagrams to chondrite (Nakamura 1974) and preliminary mantle (Sun and McDonough 1989) (Figs. 5a and 5d) have relatively high concentrations of incompatible elements, large ion lithophile elements (LILE), and light rare earth elements (LREE) and relatively low concentrations of heavy rare earth elements (HREE) and high field strength elements (HFSE), especially Ta, Nb, and Ti. Therefore, they might have a subduction-related magma origin (Goss and Kay 2009; Kovalenko et al. 2010). The parallelism of the distribution pattern of REEs, their almost constant changes, and the slope of the distribution pattern of rare earth elements are attributed to the fractional crystallization in the formation of various basic to moderate rocks. Sub-alkaline basaltic magma can also be originated from 15 to 30% partial melting of upper mantle peridotites (Green 1973; Green and Ringwood 1986) since melting at less than 10% can lead to the formation of alkaline basaltic magma (Hirschmann et al. 1999). In fact, due to the greater sensitivity of more incompatible elements to partial melting degrees, the REE pattern reduces by increasing the partial melting degrees. The parallel earth element diagrams of the rocks reveal the control of fractional crystallization and differentiation on the basaltic melt. The moderate rocks (andesitic-trachyandesite) mainly have a higher enrichment level than the continental elements, with a more dominant distinction between LREE and HREE. Severe positive anomalies of Pb and Ba indicate continental crustal contamination, and a positive Sr anomaly represents the existence of phenocryst plagioclase in the rock.

In the tectonic environment differentiation diagrams, these rocks are located in the back-arc basin (Figs. 6a and 6b). Further detailed studies represent the formation of these magmatic belt rocks in a shallow marine basin of the back-arc basin of Central Iran's main magmatic back-arc (Sarem et al. 2021). This environment is located in the main magmatic back arc of Urmia-Dokhtar (Berberian and king, 1981). The presence of the northern part of the Central Iran structural zone in the study area may suggest that the magmatic strip of Davarzan-Kahak-Abbasabad-Torud and its continuation to the south of Damghan-Semnan-Garmsar-Varamin-Qom-Saveh have all been formed in this back-arc basin. The lower La/Sm ratio is the characteristic of mantle-derived magmas (Sun and McDonough 1989), while the upper crust is characterized by a high ratio of about 6.7 (Taylor and McLennan 1981). The ratio of these elements in the basalts of the area (a mean of 4.12) indicates the lower impact of the upper crust on the evolution of these rocks.

The Sm/Yb ratio is applied to identify the origin mineralogy. The partial melting of a garnet-containing origin produces a melt with Sm/Yb > 2.5 relative to the origin (Aldanmaz et al. 2000). Thus, the ratios of these elements can reveal well the presence or absence of garnet in the magma's origin. Since the studied samples have Sm/Yb ratios of higher than 2.5, the presence of garnet in the basalt origin area is confirmed. Nb-Zr diagrams (Fig 6b) by Abu-Hamatteh (2005) were used to recognize the enrichment or non-enrichment of the origin of the studied rocks. These ratios in the preliminary mantle are about Nb/Zr = 15.71 and Y/Zr = 2.46 (Sun and McDonough, 1989). Considering the average of these ratios in the studied basaltic olivine rocks as 14.54 and 1.95, respectively, the basaltic rocks are located in the enriched mantles range on the diagrams.

The amount of crustal contamination and its role in the evolution of magmas forming the rocks in the area were determined using the trends presented by He et al. (2010) and the ratios of rare elements provided by Hart et al. (1989). The trend of analyzed samples on the diagram of Th/Nb changes versus SiO2 represents the role of differential crystallization and the involvement of crustal contamination in the evolution of the rocks (Fig 7c). Moreover, according to Hart et al. (1989), the La/Nb > 1.5 and La/Ta > 22 ratios indicate magma contamination with crustal compounds. As in this diagram, the most important factor in basaltic rocks is fractional crystallization (FC). However, by the cessation of magma in the subsurface cells and the occurrence of moderate rocks

with the cessation of magma in the subsurface chambers and the occurrence of intermediate rocks (andesite and trachyandesite), crustal contamination has also been effective in addition to differentiation.

Tchameni et al. (2006) used the diagram of Rb/Th changes against Rb to recognize differential crystallization, crustal contamination, and assimilation-differential crystallization in the rocks. In this diagram, the studied samples represent an almost ascending trend indicating the process of assimilation-fractional crystallization (AFC) in the magmatic evolution of the studied rocks. This diagram is more controlled by FC in the basaltic melts. However, by the cessation of magma and differentiation, crustal contamination has also been possible (Fig 7d). The trends marked on the figures include CC: crustal contamination, AFC: assimilation-differential crystallization, and FC: Differential crystallization.

Experimental data indicate that the K-rich magma could not form by low-degree (2-2.5%) partial melting of lherzolite at less than 2-3 GPa (70-100 km). The explanation is that it can only yield basanitic magma with SiO_2 contents inconsistent with the criteria for shoshonites (Wang et al. 1991). The enrichment of the mantle wedge in incompatible elements can be related to the following factors (Rock 1991): (1) involvement of an anomalous, metasomatized potassium-rich lithospheric mantle domain and (2) recycling of a crustal component in subduction zones (e.g., Tatsumi and Eggins, 1995; Jahn et al. 1999).

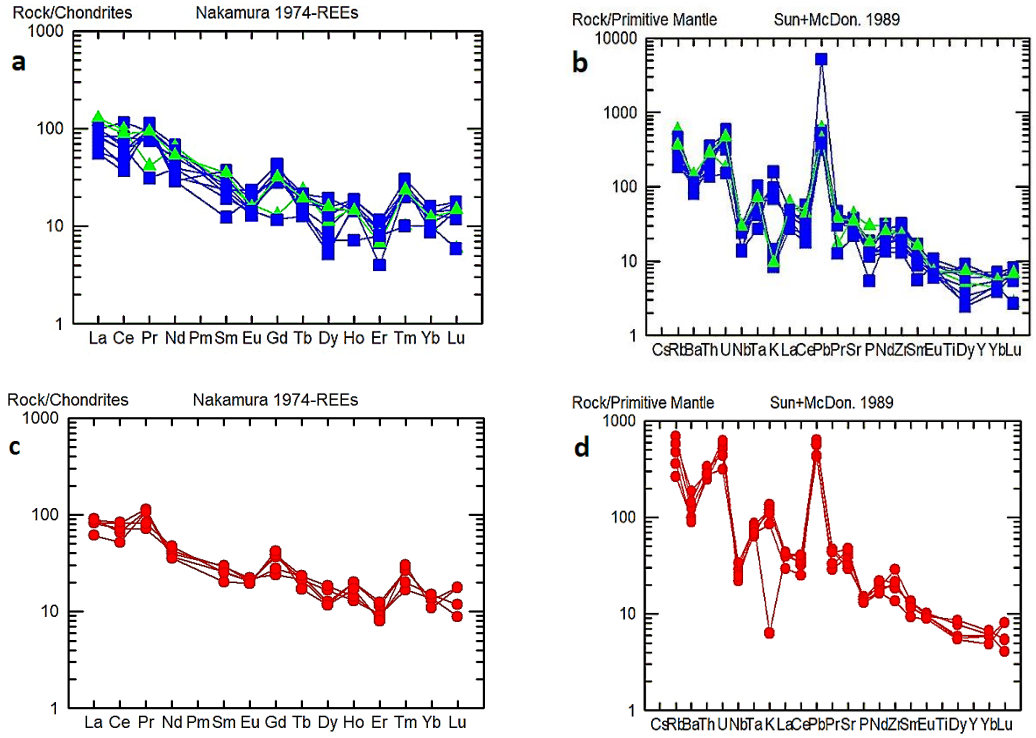

Fig 5. a) The normalized multi-element spider diagrams of andesite and trachy-andesite samples relative to the original mantle (Sun and McDonough 1989); b) The chondrite-normalized diagrams of the studied andesite and trachy-andesite samples (Nakamura 1974); c) The normalized multi-element spider diagrams of the basalt samples relative to the preliminary mantle (Sun and McDonough 1989); d) The chondrite-normalized diagram of the studied basaltic samples (Nakamura 1974).

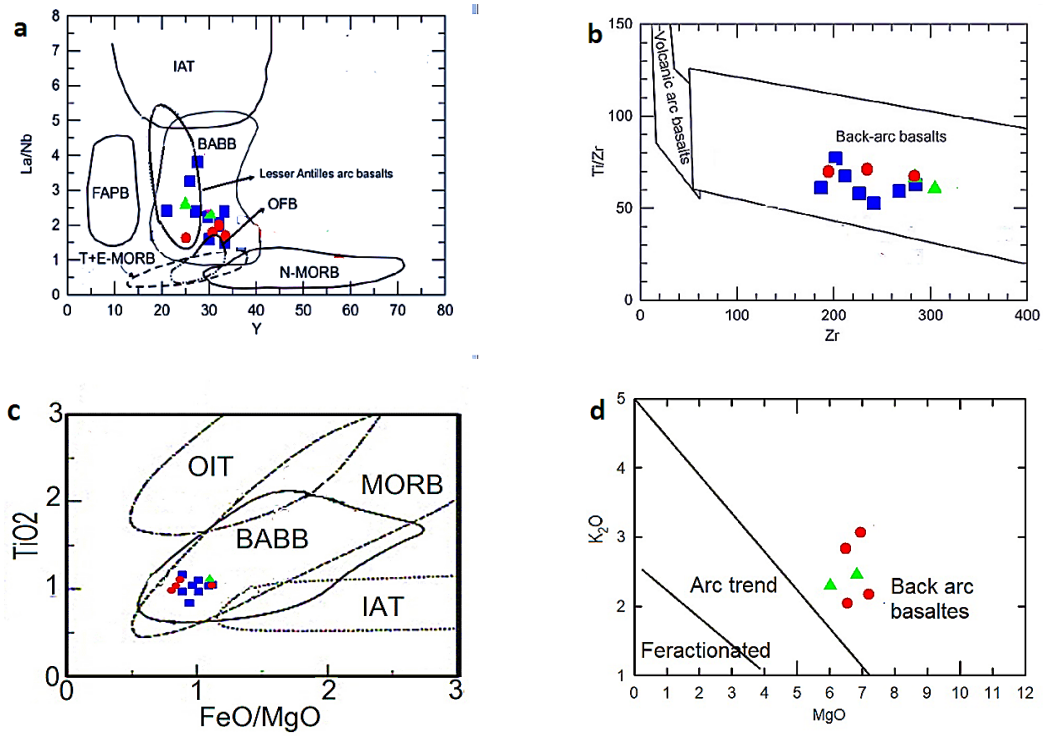

Fig 6. a) The diagram of determining the tectonic setting of basalts (Woodhead et al. 1993); b) The diagram of determining the tectonic setting of basalts and location of studied samples within the back-arc volcanic rocks (Floyd et al. 1991); c) The diagram of TiO_2-FeO/MgO (Shutoa et al. 2004); d) The diagram of Varekamp et al. (2010).

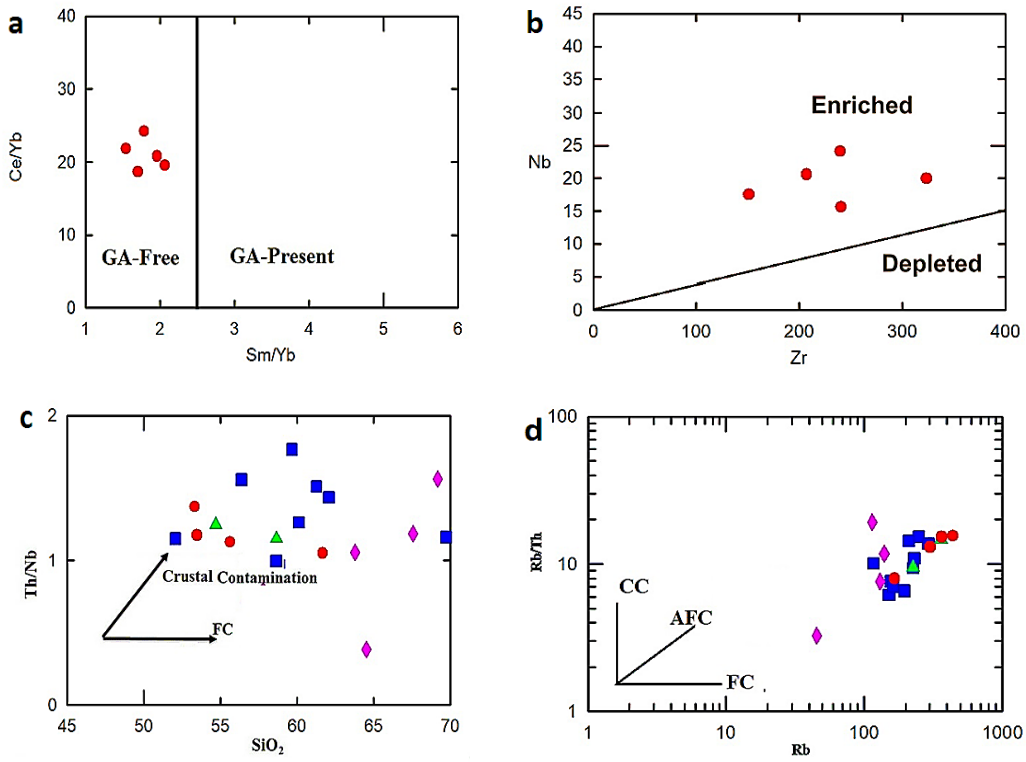

Fig 7. a) The diagram of Ce/Yb versus Sm/Yb ratios (Coban 2007); b) The diagram Nb against Zr (Abu-Hamatteh 2005); c) The graph of Th/Nb changes vis. SiO_2 to determine the amount of crustal contamination and its role in the evolution of magmas forming rocks in the area, the trends presented by He et al. (2010); d) The diagram of Rb/Th ratio changes vs. Rb (Tchameni et al. 2006).

3.2.1. Diagrams of La/Sm changes vs. Sm/Yb and Sm vs. Sm/Yb (Green 2006)

In these two diagrams (Figs 9a and 9b), the depleted MORB mantle is represented as DMM (Mckenzie and O'Nions 1995) and the preliminary mantle as PM. The melting curve (line) for spinel lherzolite (Ol53 + Opx27 + Cpx17 + sp11) and garnet peridotite (Ol60 + Opx20 + Cpx10 + GT10) was determined for both DMM and PM origins (after Aldanmaz et al. 2000). The circles on the melting curve refer to the degree of partial melting of the mantle origin. Moreover, N-MORB and E-MORB (Sun and McDonough 1989) are also represented in the figures.

3.2.2. The Zr/Nb versus La/Yb (Aldanmaz et al. 2000)

The Zr/Nb versus La/Yb diagram (Fig 9c) represents the N-MORB and E-MORB (Sun and McDonough, 1989) and MORB compounds (Niu et al. 2001). Fig 9c also shows the integrated melting process of DMM and PM. The thick lines (line) represent the partial melting degree in this figure.

Based on the presented diagrams, the basalts fall in the range of enriched mantles in line with the spinel-garnet origin of the lherzolite with the partial melting of 5 to 10%.

3.3. Tectonomagmatic pattern of formation of studied igneous rock

In the active continental margin, subduction and the completion of the oceanic crust leads to the collision of two continental plates and the initiation of an orogenic cycle. The post-collision basin normally includes a complex course.

Various tectonic models have been used to justify post-collision tension, including fracture and detachment of the subduction plate (VonBlanckenburg and Davies 1995), lithosphere scaling (Bird 1979), regression or slab rollback (Lonergan and White 1997), and local tensile strengths (Keray and Vine 1996; Einsele 2000). High-slope subduction is one of the causes of rollback that create a tensile environment. According to the experimental research, rollback and tensile basins are formed when the subduction rate is higher than the convergence rate (Schellart et al. 2002). In this case, the collision and shear stresses between the two subducting and the overriding plates are small, expanding in the surface plate of the tensile basin (Jarrard 1986; Northrup et al. 1995; Mollai et al. 2021). The main structures and forces trends in a subduction system are presented in Fig 9. Heuret and Lallemand (2005) assessed several factors controlling the formation of rollback (Fig 10).

According to the "slab rollback model", it can be stated that: (1) seaward trench motion should be a ubiquitous feature of oceanic subduction zones; (2) the older and colder a slab is, the harder it should pull down on the hinge and the faster it should rollback; and (3) back-arc extension should be associated preferentially with old slabs (Heuret and Lallemand. 2005).

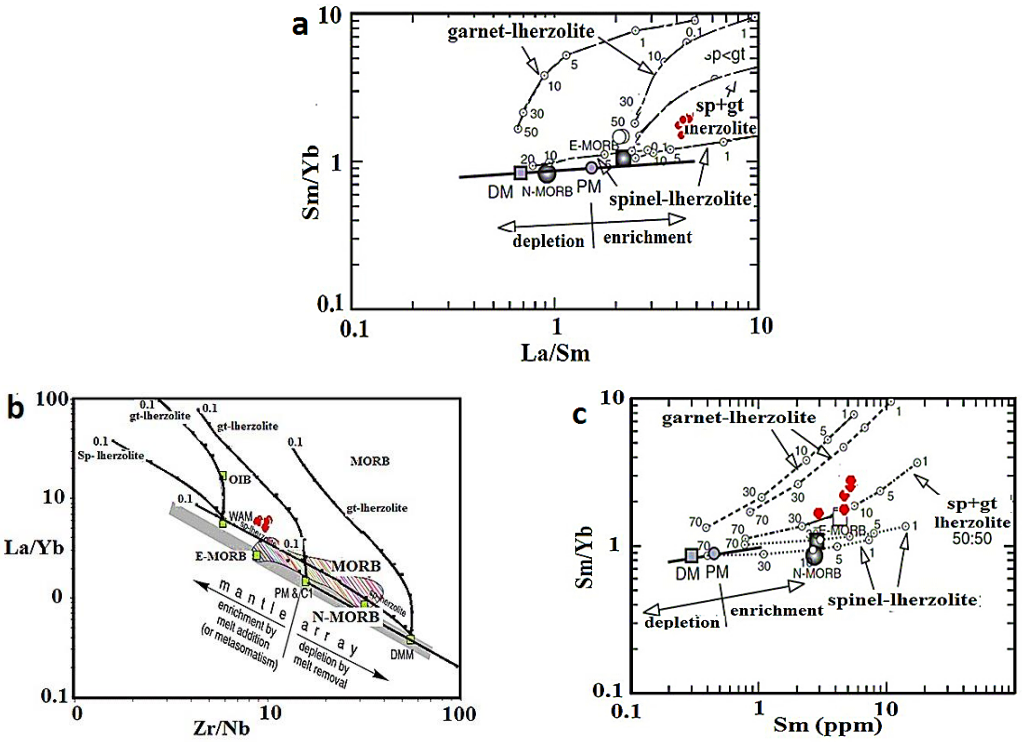

Fig 8. a) and b) The diagrams of La/Sm changes vs. Sm/Yb and Sm vs. Sm/Yb; c) The diagrams of Zr/Nb vs. La/Yb

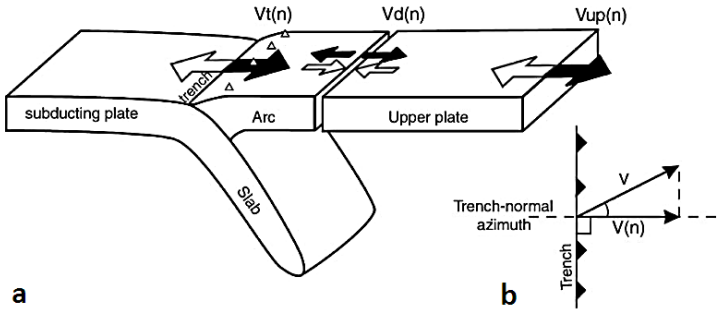

Fig. 9. a) Structural pattern of subduction zones. Vup: upper plate absolute motion, Vt: trench absolute motion, Vd: back-arc deformation rate. Grey and black arrows, respectively, refer to positive and negative velocities. b) Trench-normal components of motion estimate (Vup, Vt, or Vd)
V: rate and V (n): trench-normal component of the rate.

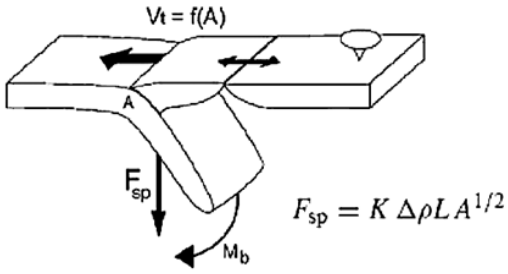

Fig 10. The formation of a rollback (Heuret and Lallemand 2005) (Abbreviations: Vup: upper sheet velocity; FSP: Compressive force of the section; Mb: bend flexural motion; Vt: lower sheet velocity A: sheet age; Δρ: density difference between sheet and mantle; L: Sheet length, K: Fixed)

Niu (2014), using the laws and physical relations, schematically examined the subduction of a young sheet with a low angle (BT 1 at time T1), in which the subduction angle increases over time (e.g., from time T1 to T2 and to T3) toward vertical under gravity.

For conceptual clarity, this research assumed the overriding plate as being "fixed", but this is not the case in practice (see Fig 12). This author also emphasized the concept and assumed the overriding plate to be continental plate/lithosphere.

Fig 12 illustrates the evolution of a subduction system from time T1 to T2 and to T3, during which the slab rolls back (Fig 11). The concept of trench retreat indicates the migration of trench seaward with time because of the gravity (dashed line in Fig 12).

The importance of the trench retreat here is the induced trench suction force (Forsyth and Uyeda 1975), as illustrated by the inset in Fig 12, which sucks/drives the overriding continental plate/lithosphere to follow the retreating trench passively (see yellow arrows in Fig 12).

The passive migration of the overriding continental plate/lithosphere in response to trench retreat/suction is the very mechanism of continental drift, whose ultimate driving force is seafloor subduction (Niu 2014).

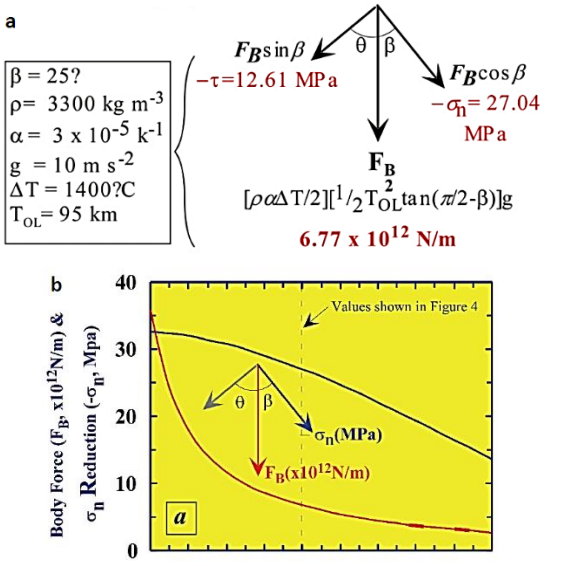

Fig 11. a) By the Stein and Stein, 1996 parameters and by considering the volume of the lithosphere of 1 m thickness defined by the triangular cross area beneath the fault plane can physical consequences of the incipient sinking of the parameters used are from Stein and Stein (1996). The physical consequences of the incipient sinking of the NOL areevaluated by considering the volume of the lithosphere of 1 m thickness defined by the triangular cross area beneath the fault plane.

b) Calculated forces and stresses as a function of the dip angle β of the fault plane across a plate of 95 km thick. Potential negative buoyancy forces (or body force; FB) at all practical dip angles of 20-45° is similar to or significantly greater than ridge push forces (~4 x 10^{12} N/m), which by itself reduces normal stress by ~15 to 30 MPa. As a result, it opens the fault plane and creates resistance-free sliding) Niu 2014).

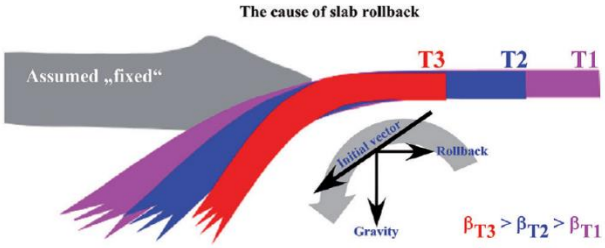

Fig 12. This picture illustrates the cause of slab rollback. Figs. 11a and 11b show that *FB* is the principal force for subduction initiation and is inversely related to the dip angle (i.e., $FB \propto -\beta$). It means that a smaller dip angle β favors subduction initiation. Once subduction begins, the slab tends to rotate vertically under gravity (βT3 > βT2 > βT1) (Niu 2014).

Cartoon illustrating trench retreat and continental drift. Under gravity, slab will roll back (Fig 12), and subduction zone will necessarily move seawards or retreat. Trenches are surface expressions of subduction zones.

Cartoon illustrating trench retreat and continental drift. Under gravity, slab will roll back and importantly, subduction zone will necessarily move seawards or retreat, which is often described as "trench retreating" because the trenches are surface expressions of subduction zones (Fig 12).

The dashed line indicates the newer position of the trench/subduction zone with time: T1→ T2→ T3. Importantly, the overriding continental plate will passively follow the retreating trench, which may be termed as the result of trench suction (Forsyth and Uyeda 1975). Thus, continental drift is a passive response to subduction, and the drifting overriding continental plate is under extension.

According to Verdel (2009), the subduction of the Neotethys oceanic lithosphere with a steep slope relative to the beneath the southern edge of central Iran has played a key role in the formation of back-arc tensile basins of central Iran. Among the important characteristics of magmas related to post-collision environments are features similar to that of subduction environments magmas. These features are reflected in some geodynamic diagrams of the region. The geochemical properties similar to subduction environments result from pre-collision metasomatism of the mantle wedge and the penetration of fluids released from the subduction edge (Pearce et al. 1990; Plat and England 1994). Various mechanisms have been proposed for mantle metasomatism. The enrichment mantle wedge over the subduction zone may be caused by the aqueous fluids derived from the dehydration process of the altered oceanic crust (Tatsumi et al. 1986; Hawkesworth et al. 1993, 1997a,b). It might also be metasomatized by partial or whole melting of subducted sediments or even the oceanic crust (Elliott et al. 1997; Foden et al. 2002). These two origins can be distinguished by some geochemical features. For

instance, rocks originating from fluids-metasomatized mantle have high values of Ba/Th, U/Th, and Sr/Th (Hawkesworth et al. 1993; Turner et al. 2005). However, magmas originating from metasomatized mantles by subducted sediments or partial or complete melts have high Th/Ce, Sr^{87}/Sr^{86}, and Th ratios (Hawkesworth et al. 1997 a,b,c).

A key feature of subduction-related mantle metasomatism is the formation of hydrous mineral phase(s) phlogopite and amphibole. The presence of phlogopite or pargasite hornblende in the source can lead to the formation of K-rich magmas (Zhang et al. 2008). Beccaluva et al. (2004) proposed that subduction-related mantle metasomatism is due to the formation of hydrous mineral phase(s) phlogopite and amphibole. The melting of a phlogopite bearing peridotite may produce potassium-rich parent magma (Müller and Groves 1997).

The melts in source with phlogopite show high Rb/Sr (> 0.1) and low Ba/Rb (< 20) (Furman and Graham 1999). Meanwhile, Ba is partitioned into phlogopite to a greater extent than Rb (Ionov et al. 1997). On the other hand, significant removal of phlogopite from the residue by (higher degree) partial melting of the veins will increase the Ba/Rb ratios (Kurt et al. 2008). The high-K samples from the Torud intermediate-basic rocks show low Ba/Rb and variably high Rb/Sr ratios, which support a low-degree partial melting of phlogopite-bearing veined lithospheric mantle source. Moreover, the studied samples have constantly high Yb concentrations exceeding 2.5 ppm and thus do not support amphibole as a residual mineral phase in the mantle source (Guo et al. 2005). However, the degree of enrichment of middle REE relative to heavy REE such as Yb depends mainly on garnet existence as a residual phase during melting because HREEs are preferentially retained by this mineral (Zhang et al. 2008).

According to geochemical data, the Eocene volcanism (Like continental arc basins) may have continued to a limited extent by the Oligocene basaltic volcanism, which is specific to back-arc basins (Verdel 2009). The formation of back-arc basins is related to the tension caused by the subduction of the oceanic plate beneath the continental lithosphere. Thus, the rocks of these areas are expected to acquire the geochemical properties of continental arc rocks. Verdel (2009) interprets this event as a modification of central Iran's origin area of the arc basalts. The resultant magmas have ascended along deep faults in the tensile zone while undergoing various petrological processes such as differential crystallization along with assimilation and crustal contamination (Fig 13). Existing calc-alkaline magmas could erupt as lava in a shallow sedimentary environment and the late Eocene-Ogocene and into red marl sediments or penetrate the lower red formation as several semi-deep masses (Fig 13).

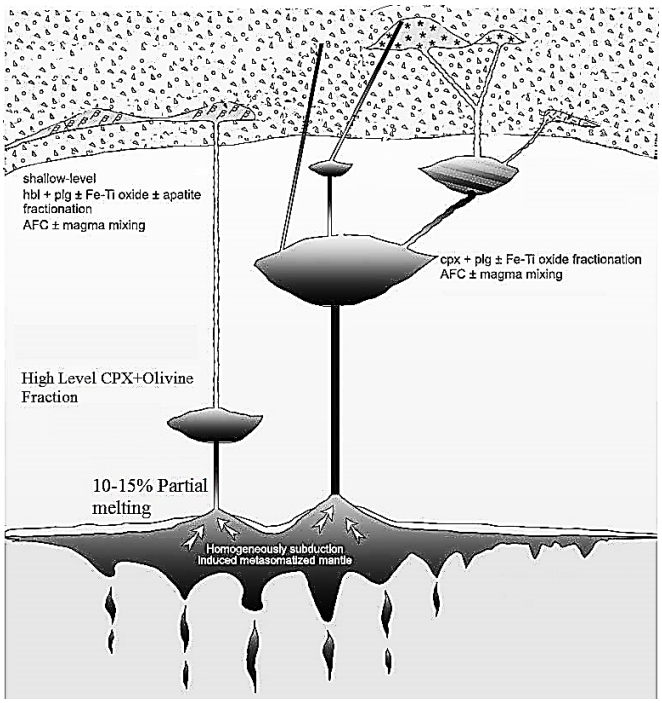

Fig 13. The schematic of the formation of alkaline magmas forming of Torud's olivine basalts to the penetration of semi-deep gabbro-diorite masses of Torud (inspired by the design of Temizel and Arslan 2008)

Table 1. Trace element concentrations of the volcanic rocks (ppm).

Sampl.	E12	E21	E23	E27	E31	E42	E43	E47	E74	E3
Ag	0.1	0.1	0.2	0.1	0.1	0.3	0.2	0.2	0.3	0.2
As	8.4	1	0.1	11.5	1	1	1	5.8	1	1
B	9.5	8.4	11.2	10.3	10.6	11.3	9.5	8.9	11.5	8
Ba	560.8	683	641	641.4	635.7	771	764.3	602.3	1003	647.1
Be	1.9	2.3	3	1.6	1.7	1.5	1.5	2	2.8	2.5
Bi	2	2	1	0.8	2.2	1.9	2.9	2	1.8	1.5
Cd	0.1	0.2	0.2	0.1	0.4	0.1	0.2	0.4	0.4	0.1
Ce	60.4	100.3	60.6	84.6	35.3	40.8	31.6	51.3	76.4	52.5
Co	24.9	24.4	6	11.5	29.1	20.7	27.6	24.8	18	20.6
Cr	25.6	60.4	30	51.4	81.7	38.1	24.5	53.5	62.3	62.1
Cu	88.6	19.2	21.1	38.7	109.1	81.5	150.9	31.7	284	30.7
Dy	3.3	5.3	2.9	3.8	6.7	1.8	5.4	4.4	5.4	5.2
Er	2.1	2.2	1.2	1.8	1.5	1.6	2.5	2.6	1.5	2.1
Eu	1.1	1.5	2.7	1.3	1	1.5	1.8	1.5	1.2	1.2
Ga	21	23.2	20.8	24.4	23.9	18.8	24.6	22.4	22.3	18.4
Gd	9.7	8.8	4.3	3.6	10.8	10.2	12	9	8.7	7.7
Ge	2	2	1.1	1.9	2.1	2	2.7	1.9	2.7	1.7
Hf	11.9	21.2	10.2	13.5	6.8	11.5	8.1	10.7	24.1	26.8
Hg	0.07	0.05	0.07	0.1	0.13	0.1	0.03	0.12	0.12	0.09
Ho	1.2	1	1.1	1.1	1	1.2	1.3	1.3	1	1
La	32.2	32.4	30.2	41.7	23.9	18.9	18.4	27.6	38.3	26.8
Li	42.3	42.9	14.7	12.9	22.5	33.8	27.1	22.2	17.4	31.7
Lu	0.5	0.5	0.2	0.2	0.6	0.5	0.6	0.5	0.5	0.4
Mn	1059	998.2	258	1284	2022	1301	1982	806.6	1176	681.5
Mo	145.4	47.1	30.5	24.5	57.6	16	28.7	58.5	134.9	66.5
Nb	17	17.1	14.6	19.9	21.3	9.8	18	18.4	21	17.2
Nd	42.7	36.7	23.5	40.9	37.2	18.2	20	18.4	33.4	24.8
Ni	14.1	21.4	2.1	18.5	22.3	9.9	12.9	19.3	19	14.8
P	1417.6	1288.7	909.6	2808.8	1294.4	1090.2	1309.7	1254.5	1702	1179.2
Pb	22.2	39.4	32.7	43.1	369	31.9	25.5	27.2	31.1	24.8
Pr	11.7	10.5	5.4	4.6	10.9	12.1	12.7	10.9	10.4	9.1
Rb	250.6	197.5	131.1	363.4	232.1	212.6	157.8	163.1	227.4	152.4
S	208	213.7	178.4	2357.2	201.9	281.4	249.4	199.6	171	177.7
Sb	4	1	0.1	4	2.6	3.4	5.2	0.8	1	0.9
Sc	15.6	20.9	9.7	15.3	27.2	13	24.1	19.5	19.7	17.7
Se	0.1	0.1	0.1	0.1	0.1	0.1	0.1	0.2	0.1	0.1
Sm	4.7	5.7	3.8	5.5	4.3	2.5	4.8	7.5	7.1	6.3
Sn	4.4	4.9	1.9	2.9	5.2	3.9	5.8	4	4.3	3.8
Sr	798.8	663.5	516.3	889.8	695.4	684.5	592.2	605.7	728	588.8
Ta	3.1	2.7	0.1	2	4.2	3.5	2.3	1.7	2.9	2.2
Tb	0.7	1	0.8	1.1	1	0.6	0.8	1	0.9	0.9
Ti	4641	6137	4085	6413	6011	3104	4799	5497	5422	5451
Th	16.4	30.2	17.3	24.8	21.3	14.8	20.7	23.2	24.1	24.7
Tl	0.7	0.9	1.3	0.9	0.9	0.8	1.2	0.9	0.8	0.8
Tm	0.7	0.7	0.3	0.3	0.8	0.8	0.9	0.7	0.7	0.6
U	10	11	3.7	3.8	12.4	12.3	12.3	8.5	9.8	6.7
V	216.1	234.8	105.4	189.8	303.6	167.5	320.3	219	244.8	191.3
Y	20.6	27	23.3	18.3	23.6	14.2	27.1	25.9	23.8	25.9
Yb	2.7	3.1	2.6	2.2	2.9	1.9	3.5	3.1	2.7	3
Zn	79.4	84.5	48.9	44.7	173.9	79.1	105.7	73.9	77.6	66.6
Zr	229.5	337.5	357.2	239.8	167.5	146.2	174.1	335	253.6	356.3

Table 1. Continued

Sampl.	E9	E25	E28	E38	E50	E65	E36	E55	E58	E79
Ag	0.1	0.1	0.1	0.2	0.2	0.1	0.1	0.2	0.2	0.2
As	6	1	69.2	14.1	1	4.7	1.8	11	8.9	3.2
B	13	8.1	8.9	11.2	13.4	8.6	9.9	8.8	9.4	14.3
Ba	690.1	628.5	871.4	1001.7	1311.9	850.9	684.1	1551.8	701.3	786.1
Be	2.5	1.8	1.8	1.6	1.4	2	3	1.5	1.4	3.2
Bi	2.2	2.3	1.5	1.5	2.6	1.8	0.7	1.4	1	0.5
Cd	0.2	0.1	1	0.5	0.3	0.1	0.2	0.5	0.3	0.1
Ce	56.8	70.3	62.4	72	44.8	71	63.5	40.5	35.2	55.6
Co	26.9	25.2	25	24.2	28.9	12.1	3	16.3	13.8	6.6
Cr	49.9	62	58.6	62.9	23.5	28.1	65.2	64.7	51.5	69.5
Cu	30.5	34.1	32.8	19.9	60.7	54	32.1	77.4	286.4	418.4
Dy	4.1	4.3	5.7	6.3	4	2	4	1.1	1.6	2.5
Er	2.6	2.8	2.1	2	1.8	0.9	2	1.4	1.2	1.8
Eu	1.6	1.6	1.7	1.6	1.5	1.1	1.9	1.4	2.1	1.1
Ga	22.3	24	24.9	22.2	26.5	24.2	19.8	19.7	22.3	20.6
Gd	10.2	10.6	6.6	7.6	11.6	8.6	2.8	6	6.1	3.2
Ge	1.7	2.1	2.1	2.1	2.3	2.2	0.9	1.6	2.4	2.6
Hf	16.6	18.5	9.7	23.5	18.6	18.5	3.2	21	13.2	8.8
Hg	0.11	0.12	0.1	0.09	0.08	0.08	0.12	0.12	0.06	0.08
Ho	1.4	1.4	0.9	1	1.2	1.1	1	0.9	1	0.5
La	30	27.2	27	29.3	20.2	27.3	32	30.1	20.1	33.4
Li	35.4	32.1	57.3	90.7	48.7	11.5	15.9	25.5	20.1	15
Lu	0.6	0.6	0.3	0.4	0.6	0.5	0.1	0.3	0.3	0.2
Mn	1033.3	1282.3	1801	1312.4	1737.4	1421.3	801.8	1417.5	878.8	426.9
Mo	81.4	78.5	36.3	69.3	93.7	53.2	89.5	32.2	52.1	244
Nb	20	15.6	20.6	24.1	17.5	9.9	8.9	11.3	15.6	10.1
Nd	25.1	23.2	26.5	29.7	22.4	31.5	32.2	28.1	17.7	24.3
Ni	15.6	21.6	27.9	25.6	12	11.8	1.7	23.7	24.9	1.9
P	1430.8	1296.1	1328.2	1336.3	1241	1768.6	704	1178.5	1174.5	518.6
Pb	39.7	44.4	30.6	30.6	40.6	37.4	19.8	27.2	25.1	27.6
Pr	12.2	12.8	8	9.1	12	8.3	3.9	7.5	7.6	3.5
Rb	166.9	227.9	302.7	439.8	366.8	295.2	45.6	140.5	114.8	117.7
S	205.6	237.3	142.2	148.9	286.5	312.4	303.3	356.6	184.2	205.2
Sb	2.5	1.4	6.9	2.6	6.2	5.3	1.7	1.7	2.8	0.6
Sc	17.7	22	26.3	29	20.3	12.5	9.3	10.9	10.1	9.4
Se	0.1	0.1	0.1	0.2	0.2	0.1	0.2	0.1	0.1	0.1
Sm	6	5.2	5.9	5.1	4.1	5.4	5.8	3.8	3	3.9
Sn	3.5	4.9	5.8	5.7	5.7	4.7	1.8	2.9	2.6	1.6
Sr	619.5	698.6	836	959.8	995.6	761.9	175	538.3	453.7	460.1
Ta	2.6	3.5	3.3	3.1	2.8	2.6	1.9	2.5	0.9	1.1
Tb	1	1.1	1	1.1	0.8	0.7	0.6	0.6	0.5	0.6
Ti	5701.6	5651.3	6357.7	6583.3	4360.8	3877.4	3169.3	2960.1	2814.6	3052.3
Th	21	24.3	23.2	28.3	24	21.6	13.9	11.9	6	11.7
Tl	1.2	0.9	0.8	0.8	1	1	0.7	1	0.9	1
Tm	0.8	0.8	0.5	0.6	0.9	0.7	0.2	0.5	0.5	0.3
U	10.8	11.3	6.6	9.2	12.9	9.4	3.5	5.6	6.3	3.2
V	194.5	281.7	321.5	356.7	273.8	168.5	45.4	130.3	115.6	44.1
Y	25.8	23.3	24.4	27.3	18.5	19.4	23.3	11.4	9.3	21.1
Yb	2.9	2.9	3	3.3	2.4	2.4	2.3	1.4	1.2	2.2
Zn	114.2	113.6	102.9	94.5	100.9	98.4	30.4	134	99.5	36.5
Zr	323.9	240.6	207.3	239.8	151.2	202	171.4	113.6	106	211.8

Table 2: Continued. Results of ICP-AES analysis for main elements of the volcanic rocks (wt %)

Sampl.	SiO_2	Al_2O_3	Fe_2O_3	FeO	CaO	MgO	Na_2O	K_2O	P_2O_5	MnO	TiO_2	SO_3	SrO
E12	58.84	18.65	2.16	4.54	7.01	2.89	2.37	2.68	0.14	0.1	0.62	0.1	0.1
E21	59.7	17.5	2.37	4.98	4.73	3.19	2.88	3.4	0.31	0.1	0.82	0.1	0.1
E23	67.59	18.02	2.15	1.45	1.54	0.82	3.69	3.99	0.2	0.1	0.61	0.1	0.1
E27	54.71	18.49	2.69	2.4	11.72	0.86	3.87	2.9	0.97	0.21	1.07	1.9	0.2
E31	55.91	18.47	2.46	5.83	5.64	4.21	3.18	2.77	0.41	0.31	0.92	0.1	0.1
E42	61.31	18.38	1.98	3.39	6.16	3.03	2.3	2.51	0.31	0.21	0.42	0.1	0.1
E43	52.09	20.29	2.3	7.33	7.01	3.35	3.14	2.93	0.42	0.31	0.73	0.1	0.1
E47	60.14	16.4	2.17	4.34	5.05	3.71	2.58	4.33	0.52	0.21	0.62	0.1	0.1
E74	58.67	17.39	2.41	4.16	7.96	2.83	2.41	2.83	0.31	0.1	0.84	0.1	0.1
E3	62.11	17.59	2.26	3.36	4.22	2.67	3.09	3.6	0.31	0.1	0.72	0.1	0.1
E9	61.68	17.24	2.28	3.81	4.57	2.6	2.7	4.05	0.31	0.1	0.73	0.1	0.1
E25	56.4	18.73	2.33	4.56	9.52	2.65	2.54	1.9	0.32	0.21	0.74	0.1	0.1
E28	55.66	18.21	2.38	5.97	5.38	4.55	3	3.62	0.31	0.21	0.72	0.1	0.1
E38	53.49	18.45	2.38	6.98	6.95	4.25	2.9	3.32	0.41	0.21	0.83	0.1	0.2
E50	53.34	20.51	2.23	7.31	5.31	4.68	2.44	2.55	0.43	0.32	0.64	0.1	0.2
E65	60.44	19.12	2.06	3.93	6.37	1.44	3.39	2.06	0.51	0.21	0.51	0.1	0.1
E36	69.18	15.71	1.98	0.75	3.33	0.62	1.56	6.14	0.21	0.1	0.42	0.1	0.1
E55	63.81	16.65	2.08	2.17	3.23	2.39	2.71	5.93	0.31	0.21	0.52	0.2	0.1
E58	64.55	16.27	1.99	2.1	4.2	2.62	4.41	2.94	0.31	0.1	0.42	0.1	0.1
E79	69.76	16.5	1.82	0	1.72	0.61	3.54	4.76	0.1	2.43	0.3	0.1	0.1

4. Conclusions

Based on petrographic and geochemical data from the Eocene rocks of the Torud area, the following conclusions were reached:

- The volcanic rocks of Torud can be subdivided into two groups: intermediate (andesite, trachyandesite, and dacitic) and basic (Alkali basalts and basalt to trachybasalt).
- The fractional crystallization (FC) process may be responsible for geochemical variations within individual suites.
- The intermediate–basic rocks have a calk-alkaline and shoshonitic nature. The high Rb/Sr with low Ba/Rb ratios suggest that their parental magma originated by partial melting of a phlogopite-bearing enriched mantle.
- Primitive mantle-normalized trace and REE patterns; higher La/Nb, Ba/Nb, and Th/La ratios; and lower Nb/La, Ba/La, and Nb/U ratios of both suites indicate that they originated from a mantle source enriched by subduction-related fluids or melts.
- The volcanic rocks of Torud formed during subduction of the Neotethyan oceanic lithosphere beneath the Central Iran Continent.
- Alkali basalts were derived from a spinel-garnet peridotite mantle source via a small degree (5-10%) of partial melting.

References

Abu-Hamatteh ZSH (2005) Geochemistry and petrogenesis of mafic magmatic rocks of the Jharol Belt, India: geodynamic implication. *Journal of Asian Earth Sciences* 25: 557–581.

Aghanabati A (2004) Geology of Iran, Publications of the Geological Survey of Iran. p. 400-586.

Aldanmaz E, Pearce JA, Thirlwall MF, Mitchell JG (2000) Petrogenetic evolution of late Cenozoic, post-collision volcanism in western Anatolia, Turkey. *Journal of Volcanology and Geothermal Research* 102(1-2):67-95.

Beccaluva L, Bianchini G, Bonadiman C, Siena F, Vaccar OC (2004) Coexisting anorogenic and subduction-related metasomatism in mantle xenoliths from the Betic Cordillera (southern Spain), *Lithos* 75: 67–87.

Berberian F, Berberian M (1981). Tectono-plutonic episodes in Iran. In: Gupta HK, Delany FM, editors. Zagros, Hindu Kush, Himalaya, Geodynamic Evolution. Geodynamic Series 3, Working Group 6. Washington, DC, USA: AGU, pp. 5–32.

Berberian M, king GCP (1981) Towards a paleogeography and tectonic evolution of Iran *Canadian Journal of Earth Science* 18:210-265.

Bin Z, Meiyin D (2010) Geological setting of Garmsar block, Iran. *International Conference on Challenges in Environmental Science and Computer Engineering* 2:433-437

Bird P (1979) Continental delamination and the Colorado Plateau, *Journal of Geophysical Research* 84: 7561–7571.

Blundy J, Cashman K (2005) Rapid decompression-driven crystallization recorded by melt inclusions from Mount St, Helens Volcano. *Geology* 33 (10): 793-796.

Coban H (2007) Basalt magma genesis and fractionation in collision-and extension related provinces: A comparison between eastern, central and western Anatolia. *Earth Science Reviews* 80: 219 – 238.

Davoudzadeh M (1997) Iran. In: Moores EM, Fairbridge, RW, Eds, Encyclopedia of European and Asian Regional Geology, Encyclopedia of Earth Sciences Series, *Chapman and Hall*, London.

Einsele G (2000) Sedimentary Basins. Evolution, Facies and Sediment Budget. Second edition. *Springer*-Verlag. Berlin. 792 p.

Elliott T, Planck T, Zindler A, White W, Bourdon B (1997) Element transport from slab to volcanic front at the Mariana arc, *Journal of Geophysical Research* 102:14991-15019.

Eshraghi PS, AS (2006) Report on the Geological Map 1:100000 Moaleman.

Floyd PA, Kelling G, Gocken SL, Gocken N (1991) Geochemistry and tectonic environment of basaltic rocks from the Miss ophiolitic melange, south Turkey, *Chemical Geology* 89: 263-280.

Foden J, HwanSong S, Turner S, Elburga M, Smitha BPB, Steldtad V, Penglisa V (2002) Geochemical evolution of lithospheric mantle beneath S.E. South Australia, *Jouran of Chemical Geology* 182: 663-695.

Forsyth D, Uyeda S (1975) On the relative importance of the driving forces of plate motion, *Geophysical Journal International* 43: 163–200.

Furman T, Graham D (1999) Erosion of lithospheric mantle beneath the East African Rift system: geochemical evidence from the Kivu volcanic province. *Lithos* 48: 237–262.

Ghaffari M, Rashidnejad-Omran N, Dabiri R, Chen B, Santos JF. (2013) Mafic–intermediate plutonic rocks of the Salmas area, northwestern Iran: their source and petrogenesis significance. *International Geology Review* 55(16):2016-29.

Ghaffari M, Rashidnejad-Omran N, Dabiri R, Santos JF, Mata J, Buchs D, McDonald I, Appel P, Garbe-Schönberg D. (2015) Interaction between felsic and mafic magmas in the Salmas intrusive complex, Northwestern Iran: Constraints from petrography and geochemistry. *Journal of Asian Earth Sciences* 111:440-58.

Gile HA, Boni M, Balssone G, Allen CR, Banks D, Moore F (2006) Marble-hosted sulfide ores in the Angouran Zn–(Pb–Ag) deposit, NW Iran: interaction of sedimentary brines with a metamorphic core complex. *Mineralium Deposita* 41: 1-16.

Ginibre C, Kronz A, Wörner G (2002) High-resolution quantitative imaging of plagioclase composition using accumulated backscattered electron images: new constraints on oscillatory zoning, *Contributions to Mineralogy and Petrology* 142: 436-448.

Goss AR, Kay SM (2009) Extreme high field strength element (HFSE) depletion and near-chondritic Nb/Ta ratios in Central Andean adakite-like lavas (~ 28° S,~ 68° W) *Earth and Planetary Science Letters* 279 (1): 97-109.

Green DH (1973) Experimental mantle studies on a model upper mantle composition under water-saturated and water-unsaturated conditions, *Earth and Planetary Science Letters* 19: 37-53.

Green L. Nathan (2006) Influence of slab thermal structure on basalt source regions and melting conditions: REE and HFSE constraints from the Garibaldi volcanic belt, northern Cascadia subduction system, *Lithos* 87: 23-49.

Green TH, Ringwood AE (1986) Genesis of the calc-alkaline igneous rock suite. *Contributions to Mineralogy and Petrology* 18:105-162.

Guo Z, Hertogen J, Liu J, Pasteels P, Boven A, Punzalan L, He H, Luo X, Zhang W (2005) Potassic magmatism in Western Sichuan and Yunnan provinces, SE Tibet, China: petrological and geochemical constraints on petrogenesis, *Journal of Petrology* 46: 33-78.

Hastie AR, Kerr AC, Pearce JA, Mitchell SF (2007) Classification of AlteredVolcanic Island Arc Rocks using ImmobileTrace Elements: Development of theTh-Co Discrimination Diagram, *Journal of Petrology* 48:2341-2357.

Hawkesworth C, Turner S, Peate D, McDermott F, van Calsteren P (1997a) Elemental U and Th variations in island arc rocks: implications for Useries isotopes. *Chemical Geology* 139: 207-221.

Hawkesworth CJ, Gallagher K, Hergt JM, McDermott F (1993) Mantle and slab contributions in arc magmas, *Annual Review of Earth and Planetary Sciences* 21: 175-204.

Hawkesworth CJ, Turner SP, McDermott F, Peate DW, van Calsteren P (1997,c) U-Th isotopes in arc magmas: implications for element transfer from the subducted crust, *Science* 276: 551-555.

He Q, Xiaoa L, Baltab B, Gao R, Chen J (2010) Variety and complexity of the Late-Permian Emeishan basalts: Reappraisal of plume-lithosphere interaction processes, *Lithos* 119: 91-107.

Heuret A, Lallemand S (2005) Plate motions, slab dynamics and back-arc deformation, *Physics of The Earth and Planetary Interiors* 149: 31-51.

Hirschmann MM, Asimow PD, Ghiorso MS, Stolper EM (1999) Calculation of Peridotite Partial Melting from Thermodynamic Models of Minerals and Melts. III. Controls on Isobaric Melt Production and the

Effect of Water on Melt Production, *Journal of Petrology* 40: 831-851.

Mollai H, Dabiri R, Torshizian, Habib Allah, Pe-piper G, Wang WE. (2021) Upper Neoproterozoic garnet-bearing granites in the Zeber-Kuh region from east central Iran micro plate: Implications for the magmatic evolution in the northern margin of Gondwanaland. *Geologica Carpathica* 72(6):461-81.

Hooshmandzadeh AS, Alavi M, Haghipor AS (1357) geological evolution of the phenomenon TORUD (from the Precambrian to the present Covenant), published by the Geological Survey, 138 p.

Humphreys MCS, Blundy JD, Sparks SJ (2006) Magma evolution and opensystem processes at shiveluch volcano: insights from phenocryst zoning, *Journal of Petrology* 47 (12): 2303-2334.

Ionov DA, Griffin WI, o'reilly SY (1997) Volatile-bearing minerals and lithophile trace elements in the upper mantle, *Chemical Geology* 141: 153-184.

Irvine TN, Baragar WRA (1971) A guide to chemical classification of the common volcanic rocks. *Canadian Journal of Earth Sciences* 8: 523-548.

Jahn BM, Wu F, Lo CH, Tsa ICH (1999) Crust–mantle interaction induced by deep subduction of the continental crust: geochemical and Sr–Nd isotopic evidence from post-collisional mafic–ultramafic intrusions of the northern Dabie Complex, central China. *Chemical Geology* 157: 119-146.

Jarrard RD (1986) Relations among subduction parameters, *Reviews of Geophysics* 24(2):217-284.

Jung D, Keller J, Khorasani R, Marcks C, Baumann A, Horn P (1984) Petrology of the Tertiary magmatic activity in the northern Lut area, east Iran, Neues Jahrb, *Neues Jahrbuch für Geologie und Paläontologie - Abhandlungen, Band* 160: 417-467.

Kasmin VG, Tikhonova NF (2008) Cretaceous–Paleogene Back-Arc Basins in the Iran–Afghanistan–Pamirs Segment of the Eurasian Active Margin. *Doklady Earth Sciences* 422(7):1018-1020.

Keray P, Vine FJ (1996) Global Tectonics. Blackwell Science ,Oxford.

Kovalenko VI, Naumov VB, Girnis AV, Dorofeeva VA, Yarmolyuk VV (2010) verage Composition of Basic Magmas and Mantle Sources of Island Arcs and Active Continental Margins Estimated from the Data on Melt Inclusions and Quenched Glasses of Rock, *Journal of Petrology* 18:1-26.

Kurt MA, Alpaslan MC, Göncüoğlu MC, Temel A (2008) Geochemistry of late stage medium to high-K calcalkaline and shoshonitic dykes in the Ulukişla Basin (Central Anatolia, Turkey): petrogenesis and tectonic setting, *Geochemistry International* 46:1145–1163.

Le Roex AP, Dick HJB, Erlank AJ, Reid AM, Frey FA, Hart SR (1983) Geochemistry, mineralogy and petrogenesis of lavas erupted along the south west Indian ridge between the Bouvet triple junction and 11 degrees east, *Journal of Petrology* 24: 267-318.

LeBas MJ, LeMaitre RW, Streckeisen A, Zanettin B (1986) A chemical classification of volcanic rocks based on the total alkali-silica diagram, *Journal of Petrology* 27:745-750

Lonergan L, White N (1997) Origin of the Betic-Rir mountion belt, *Tectonic* 16(3):504-522,

Mckenzie DP, ONiins RK (1995) The source regions of ocean island basalts, *Journal of Petrology* 36: 133-159.

Meng L, Li Zh, Chen H, Li X, Wang X (2012) Geochronological and geochemical results from Mesozoic basalts in southern South China Block support thefl at-slab subduction model. *Lithos* 132-133: 127-140.

Middelmost EAK (1994) Naming materials in the magma /igneous rock system .Longman Groun u .k., 73-86.

Morrison GW (1980) Characteristics and tectonic setting of the shoshonite rock association. *Lithos* 13: 97–108.

Müller D, Groves DI (1997) Potassic Igneous Rocks and Associated Gold–Copper Mineralization. 3rd edition, Springer-Verlag, Berlin 1–238.

Nakamura N (1974) Determination of REE, Ba, Fe, Mg, Na and K in carbonaceous and ordinary chondrites, *Geochimica et Cosmochimica Acta* 38:757-775.

Nelson ST, Montana A (1992) sieve – textured plagioclase in volcanic rocks produsd by rapid decompression. *American Mineralogist* 77: 1242-1249.

Niu Y (2014) Geological understanding of plate tectonics: Basic concepts, illustrations, examples and new perspectives.

Niu Y, Bidaeu D, He`kinian R, Batiza R (2001) Mantle compositional control on the extent of mantle melting, crust production,gravity anomaly, ridge morphology, and ridgesegmentation: a case study at the mid-Atlantic ridge 33–358N, *Earth and Planetary Science Letters* 186:383-399.

Northrup CJ, Royden LH, Burchfiel BC (1995) Motion of the Pacific Plate Relative to Eurasia and Its Potential Relation to Cenozoic Extension Along the Eastern Margin of Eurasia. *Geology* 23(8): 719-722.

Peccerillo A (1992) Potassic and ultrapotassic rocks: compositional characteristics, petrogenesis, and geologic significance. *Episodes* 15: 243–251.

Plat IP, England PC (1994) Convective removal of lithosphere beneath mountain belts: thermal and mechanical consequences. *American Jourmal of Science* 294: 307-336.

Reuter M, Piller WE, Harzhauser M. Mandic O, Berning B (2007) The Oligo-Miocene Qom Formation (Iran): evidence for an early Burdigalian restriction of the Tethyan Seaway and closure of its Iranian gateways, *International Journal of Earth Sciences* 98(3):627-650

Rock NMS (1991) Lamprophyres. Blackie, London, pp 1–285.

Sarem MN, Abedini MV, Dabiri R, Ansari MR. (2021) Geochemistry and petrogenesis of basic Paleogene volcanic rocks in Alamut region, Alborz Mountain, north of Iran. *Earth Sciences Research Journal* 25(2):237-45.

Schellart WP, Lister GS, Jessell MW (2002) Analogue modeling of assymetrical back-arc extension, Journal *of the Virtual Explorer* 7:25-42.

Shelly D (1993) Igneous and metamorphic rocks under microscope classification features, microstructures and mineral preferred orientations. Chapman & Hall, London. PP 405.

Shutoa K, Hiraharab Y, Ishimotob H, Aokic A, Jinbod A, Gotoe Y (2004) Sr and Nd isotopic compositions of the magma source beneath north Hokkaido, Japan: comparison with the back-arc side in the NE Japan arc. *Journal of Volcanology and Geothermal Research* 134: 57-75.

Singer BS, Dungan MA, Layn GD (1995) Textures and Sr, Ba, Mg, Fe, K, and Ti compositional profiles in volcanic plagioclase: clues to the dynamics of calcalkaline magma chambers. *American Mineralogist* 80: 776-798.

Stein S, Stein CA (1996) Thermo-mechanical evolution of oceanic lithosphere: Implications for the subduction processes and deep earthquake. – In: Bebout, G.E. Scholl, D.W., Kirby, S.H. & Platt, J.P. (eds), Subduction top to bottom. – Am. Geophys. *Union Monogr* 96:1–17.

Stewart ML, Pearce TH (2004) Sieve-textured plagioclase in dacitic magma: Interference imaging results. *American Mineralogist* 89: 348-351.

Sun SS, McDonough WF (1989) A chemical and isotopic systematics of oceanic basalts: Implication for mantle composition and processes. In: Saunders AD, Norry MJ, (eds). Magmatism in oceanic basins. *Geological Society London Special Publications* 42. 313-345.

Talusani VR (2010) Bimodal tholeiitic and mildly alkalic basalts from Bhir area, central Deccan Volcanic Province, India: Geochemistry and petrogenesis, *Journal of Volcanology and Geothermal Research* 189: 278-290.

Tatsumi Y, Eggins S (1995) Subduction Zone Magmatism. *Blackwell*, Cambridge 1–211.

Tatsumi Y, Hamilton DL, Nesbitt RW (1986) Chemical characteristics of fluid phase released from a subducted lithosphere and origin of arc magmas: Evidencefrom high-pressure experiments and natural rocks: *Journal of Volcanology and Geothermal Research* 29:293-309.

Taylor SR, McLennan SM (1981) The composition and evolution of the continental crust: rare earth element evidence from sedimentary rocks, *Philosophical Transactions of the Royal Society of London* 301:381-399.

Tchameni R, Pouclet A, Penay J, Ganwa AA, Toteu SF (2006) Petrography and geochemistry of the Ngaondere Pan – African granitoids in Central North Cameroon: Implication for their sources and geological setting, *Journal of African Earth Sciences* 44:511-529.

Temizel I, Arslan M (2008) Petrology and geochemistry of Tertiary volcanic rocks from the-Ikizce (Ordu) area, NE Turkey: Implications for the evolution of the eastern Pontide paleo-magmatic arc, *Journal of Asian Earth Sciance* 31:439-463.

Turner Rh Mulhern B, Crisp R (2005) Impairment of executive abilities following a social category prime, *current research in social psychology* 11:29-38.

Varekamp JC, Hesse A, Mandeville CW (2010) Back-arc basalts from the Loncopue graben (Province of Neuquen, Argentina), *Journal of Volcanology and Geothermal Research* 197: 313-328.

Verdel Ch (2009) Cenozoic geology of Iran: An intergrated study of extentional tectonics and related volcanism. In partial fulfillment of the requirement for the degree of doctor of philosophy. California institute of technology Pasadena, California, pp. 287.

Verdel Ch, Wernicke BP, Hassanzadeh J, Guest B (2011) A Paleogene extensional arc flare-up in Iran, *Tectonics* 30(3):1-20.

Vernon RH (2004) A Practical guide to rock microstructure.Cambridge, 594p.

VonBlanckenburg F, Davies JH (1995) Slab breakoff: A model for syncollisional magmatism and tectonics in the Alps, *Tectonics* 14(1):120–131.

Wang D, Zhou J, Qiu J (1991) The research status of shoshonitic series rocks. J Nanjing Univ (Earth Science) 4:321–328.

Widdowson HG (1991) Aspects of Language Teaching. Oxford: OUP (1996). Teaching Language as Communication. Oxford: OUP. p 160.

Widdowson M, Pringle MS, Fernandez OA (2000) A post K-T Boundary (Early Palaeocene) age for Deccan-type feeder dykes, Goa, India, *Journal of Petrology* 41:1177-1194.

Woodhead J, Eggins S, Gamble J (1993) High-field strength and transition element systematics in island arc and back-arc basin basalts: evidence for multiphase melt extraction.

Yazdi A, Ashja-Ardalan A, Emami MH, Dabiri R, Foudazi M (2019) Magmatic interactions as recorded in plagioclase phenocrysts of quaternary volcanics in SE Bam (SE Iran), *Iranian Journal of Earth Sciences*, 11(3): 215-224.

Yazdi A, ShahHoseini E, Razavi R (2016) AMS, A method for determining magma flow in Dykes (Case study: Andesite Dyke). *Research Journal of Applied Sciences*, 11(3), 62-67

Zhang Z, Xiao X, Wang J, Wang Y, Kusky TM (2008) Post-collisional Plio- Pleistocene shoshonitic volcanism in the western Kunlun Mountains, NW China: geochemical constraints on mantle source characteristics and petrogenesis, *Journal of Asian Earth Sciences* 31:379-403.